J. Fluid Mech. (1975), *vol.* 69, *part* 2, *pp.* 283–304
Printed in Great Britain

On transition in a pipe. Part 2. The equilibrium puff

By I. WYGNANSKI, M. SOKOLOV AND D. FRIEDMAN
School of Engineering, Tel-Aviv University, Ramat-Aviv, Israel

(Received 20 May 1974)

Conditionally sampled hot-wire measurements were taken in a pipe at low Reynolds numbers ($2700 > Re > 2000$) corresponding to the onset of turbulence as a result of a large perturbation in the flow. This type of transition gives rise to a turbulent puff which maintains itself indefinitely at around $Re = 2200$. The structure of puffs was investigated in some detail and was found to be very different from the structure of fully developed turbulent pipe flow. Nevertheless, it is independent of the character of the disturbance which created it. The purpose of the study was to gain some insight into the mechanism of transition in a pipe.

1. Introduction

Two different kinds of intermittently turbulent regions were discovered in transitional pipe flow at the very outset of the investigation. We have called them puffs and slugs. Slugs are caused by the instability of the boundary layer to small disturbances in the inlet region of the pipe. Puffs are generated by large disturbances at the inlet. The origin of puffs and slugs, the range of Reynolds numbers in which they occur, and the flow field in a turbulent slug were all discussed in a previous paper (Wygnanski & Champagne 1973, henceforth referred to as W & C).

Puffs were observed in the range $2000 \leqslant Re \leqslant 2700$ only when the flow entering the pipe was disturbed beyond a certain threshold. The entire region in the neighbourhood of the inlet was turbulent. The gross behaviour of a puff at large distances from the inlet was independent of the disturbance which generated it. Oscillograms of hot-wire traces (W & C, figures 3 and 4) indicated the following.

(i) All puffs at the same Re are of equal length.

(ii) The turbulent activity in a puff is strongest in the central region of the pipe rather than near the walls.

(iii) The turbulent intensity increases gradually towards the rear of the puff and attains a maximum at the trailing edge.

(iv) There is no clear interface between the turbulent and non-turbulent zones near the leading edge of a puff. It was even difficult to determine the location of the trailing edge of a puff near the wall of the pipe.

(v) The velocity of a puff is approximately equal to the spatial average velocity in the pipe ($\overline{U}$ = volume flow/cross-sectional area).

All the observations mentioned above were made with a stationary disturbance like an orifice plate placed at the inlet of the pipe. The appearance of the puffs was random in time and no information was available on the response of the flow to a single perturbation. Valerani (1964) introduced single and periodic disturbances into the flow and watched the response of the system at the exit of the pipe. He observed that for a single perturbation there are three possible responses of the system.

(i) The flow in the pipe remains laminar for $Re < 2000$.

(ii) The pipe contains a train of turbulent regions interspersed by laminar fluid for $2100 < Re < 2500$.

(iii) A single turbulent region emerges as a response to a single perturbation for $Re > 2500$.

Valerani concluded that in the intermediate range of Re a turbulent region initially grows and then splits into a train of smaller turbulent regions (see also Lindgren 1957). There was no information about the character of the emerging regions. Presumably they resemble turbulent puffs because they occur in the same range of Re as puffs do; however, this fact had to be established. Furthermore the mechanism of splitting and possible recombination at higher Re is not understood.

In order to establish the path which the flow takes as it becomes fully turbulent at low Re (≈ 3000), we must know how puffs grow, split and possibly recombine or change their identity in the process. In attempting to answer these questions one must start by quantitatively defining what a turbulent puff is. It is the purpose of the present paper to provide adequate information about the equilibrium puff, i.e. one which does not grow, split or shrink as it travels through the pipe. This type of puff will serve in future work as a reference for comparison with non-equilibrium puffs, by which some further insight may be gained into the mechanism of transition in a pipe.

2. Apparatus and instrumentation

The basic flow apparatus was described in W & C and is shown in figure 1. A disturbance generator was added in order to study the response of the flow to a single strong disturbance for $2000 \leqslant Re \leqslant 3500$. In the configuration studied the flow is laminar provided that $Re \leqslant 17\,500$ but it is not stable to large disturbances for $Re > 2000$. The large difference between the natural transition Reynolds number and the artificially triggered transition Reynolds number ensured that no spurious turbulent bursts occurred.

Several attempts were made to create a single clean pulse of sufficient strength to trigger a turbulent puff at a Reynolds number of 2000. Although a capacitive-discharge spark generator produced a turbulent slug at $Re = 10\,000$ a very strong spark is required at lower Reynolds numbers. Breslin (1970) triggered turbulence by means of a mechanical device which consisted of a funnel covered with a Mylar membrane. A hammer caused the flow disturbance by impinging on

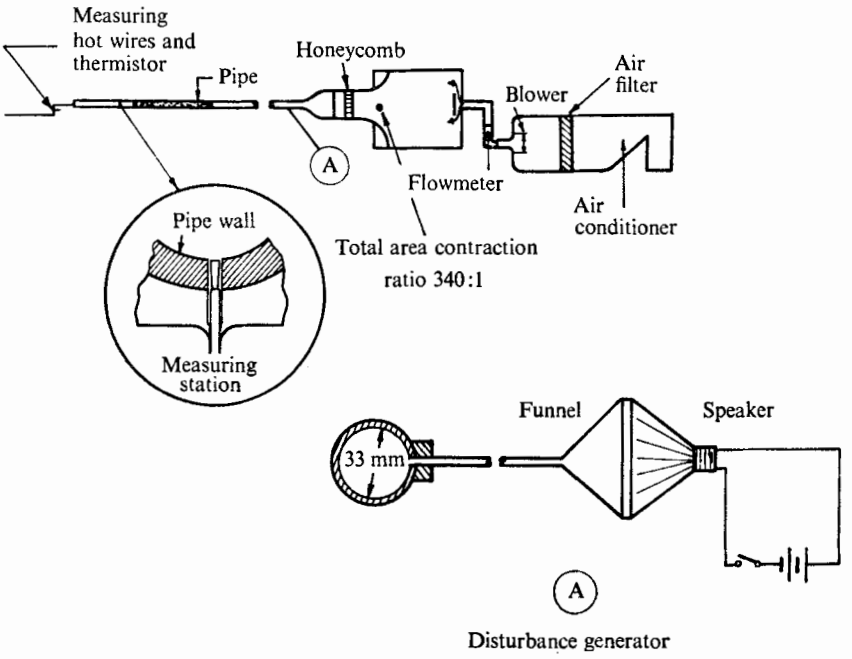

FIGURE 1. A schematic drawing of the apparatus and disturbance generator.

the membrane. A similar mechanism was built, but the results were not entirely satisfactory because of membrane vibrations, which produced secondary impulses. These impulses could give rise to additional turbulent puffs at some critical Reynolds numbers.

A satisfactory solution was found when a speaker was placed on the funnel and was activated by a d.c. voltage step (figure 1*a*). The motion of the speaker produced a small jet (1 mm in diameter) normal to the pipe flow, which provided the perturbation necessary to trigger turbulence. The applied voltage was maintained until the turbulent puff had left the pipe in order to prevent any contaminating disturbance.

Hot wires were embedded in the surface of the pipe to provide some statistical data about the flow. Other measurements were made near the exit plane using hot wires to traverse the flow radially. The hot-wire equipment has been described in detail in W & C.

Turbulent intensities were measured by passing the signal through a high-pass filter. The low frequency cut-off was experimentally chosen to block the slow changes in the mean velocity observed as a puff passes the probe, while passing most of the turbulent fluctuations. In most cases changing the cut-off frequency from 4 to 12 Hz did not significantly change the turbulent intensity, i.e. $1 > u'^2(12\text{ Hz} - 2000\text{ Hz})/u'^2(4\text{ Hz} - 2000\text{ Hz}) \geqslant 0{\cdot}95$; see also W & C.

3. Acquisition and processing of puff data

From a data-acquisition viewpoint, the main difficulty in working with a puff is synchronization. The velocity wave forms have no definite point of onset which can be used to trigger the start of recording and the trailing edge is ragged and cannot directly be used (e.g. by a threshold criterion) to define a reference point in time for aligning the wave forms for ensemble averaging. The initiation time of the loudspeaker pulse was also found not to be an accurate reference, owing to small but significant fluctuations in the propagation delay (15–20 s) of the puff along the pipe.

In this work all data recording and analysis was done digitally, using a small computer (Varian 620/i) connected on-line to the experiment through a 12-bit analog-to-digital converter (full-scale range = 4096 levels). The puff wave form was synchronized in two stages. For initial acquisition, the low-passed version of the total signal, as measured by a separate reference probe which remained on-axis, was used to give a rough location of the trailing edge of the puff. This was later refined by visually inspecting the recorded velocity wave forms for each puff on an $X-Y$ oscilloscope display driven by the computer, and manually setting a marker at the point in time judged to be the true trailing interface of the puff as seen by the cross-wire probe (figure 2, plate 1).

The acquisition process was performed as follows. A computer program was written to digitize continuously either two or three signals (an output of a single wire by which the velocity U was measured, or the outputs of a cross-wire, in addition to the d.c. component used for synchronization) at a rate of 5000 samples/s per channel. The sampling rate was more than adequate since all turbulent fluctuations were found to have negligible energy at frequencies higher than 1000 Hz. The cross-wire signals were first low-pass filtered at 2000 Hz to eliminate frequency aliasing. The sampled values for these two cross-wire channels were stored in a memory array of 2×6000 locations, so that, whenever the array became full, the address counter was reset back to the beginning of the array and the process repeated, overwriting the previously stored data. In this way a history of the preceding 1·2 s for the two channels was always maintained in memory. The program meanwhile tested the d.c. level on the third channel relative to a preset threshold. When the signal fell and rose again, indicating the passage of a puff, the program continued digitizing for a further interval (e.g. 10 ms) and then stopped, leaving in memory the puff wave forms for the cross-wire probe, framed in the 'window' of 1·2 s. The captured wave forms could be inspected on the $X-Y$ display to verify that proper triggering had occurred, and finally written out on digital tape for long-term storage.

Prior to analysis, the data recorded at a single probe station were copied from tape to disc memory for quicker working access. In doing this, the two probe channels were matrixed to give u' and v' as the sum and difference respectively.

Another program was written to read puffs one by one from the disc and display u', v', du'/dt or dv'/dt under manual selection by the user. By means of a potentiometer connected to the analog-to-digital converter, the user could input to the program a variable d.c. level, which was used to position a vertical cursor

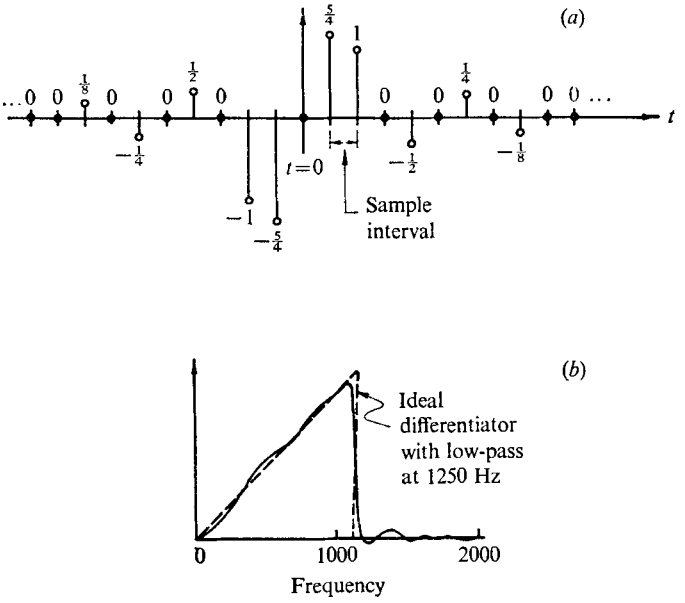

FIGURE 4. Differentiation function used in digital averaging. (*a*) Filter weighting function. (*b*) Frequency function.

line on the display. Alternatively, the cursor line could be held stationary in the centre of the screen and the wave form (time-expanded) moved left or right, giving the effect of viewing the wave form through a moveable window 160 ms wide. In this way the user could position the cursor at the point on the time axis judged to represent the trailing interface of the puff, and record the cursor location as a number stored in memory (figure 2). In later ensemble averaging, the signals were shifted to bring their respective cursor locations into mutual alignment.

After inspecting many puffs, it became apparent that the trailing interface could not always be located accurately from the signals u', v', du'/dt and dv'/dt directly, owing to the variety of wave shapes observed. The function

$$(du'/dt)^2\,(dv'/dt)^2$$

was suggested as one to which a simple threshold criterion could be applied. However, it was noted that the logarithm of this function, expressed as

$$\log(du'/dt) + \log(dv'/dt),$$

would have the advantage of showing the full dynamic range of activity. As illustrated at the bottom of figure 3 (plate 2), this function has two plateaus, one indicating the level of the background noise and the other the level of the turbulent activity. The trailing interface may be defined as the point at which the signal drops, for the last time, to one decade below its mean turbulent value.

With the refined time alignment provided by the cursor program, ensemble averages of u'^2, v'^2, $(du'/dt)^2$, $(dv'/dt)^2$ and $\overline{u'v'}$ could be calculated with high resolution in time. Furthermore, histograms of the cumulative distribution of

cursor locations for each probe station were made, to allow the trailing interface of the puff to be mapped by delay relative to the on-axis station used for synchronizing the data recording operation.

It is estimated that the accuracy of the determination of the trailing edge in the central region of the pipe was better than 0·003 s, corresponding to a spatial resolution of approximately 0·1 in.

The derivative was calculated by a symmetrical (zero phase shift) digital filtering operation which incorporated a further low-pass at 1250 Hz to reduce the effect of quantization noise. Figure 4 shows the filter weighting function and its Fourier transform in frequency. The filter function was chosen as a trade-off among (i) speed of computation in view of the large volume of data involved, (ii) accuracy of approximation to an ideal differentiator, and (iii) reduction of quantizing noise through averaging the effect at several sample points. Note that the coefficients of the weighting function are based on negative powers of 2, allowing the computation to be done using addition and shifting operations only, without multiplication.

The calculated averages were plotted on an analog X–Y plotter driven by analog output from the computer. Additional smoothing was applied using a weighting function of form $\exp(-|k\Delta t|)$.

A check on the digital averaging was made by generating an equivalent analog average of $(du'/dt)^2$ for one station. The signals u' for consecutive puffs were reproduced as analog output from the computer, and passed, in order, through a 1250 Hz low-pass filter, an analog differentiator, a squarer and a P.A.R. (model TDH-9) 100-channel wave-form eductor. The resulting plot closely resembled the computed average, with very minor discrepancies easily attributable to (i) phase shift in the analog low-pass filter, (ii) the more ideal characteristic of the analog differentiator, and (iii) the inferior resolution of the eductor, compared with the 2500 sample points used in the final digitally computed average.

4. Results and discussion

4.1. *Preliminary tests establishing the existence of an equilibrium puff*

Initial trials were run using three hot-wire probes placed flush with the inner surface of the pipe at various distances from the inlet, with a fourth sensor at the centre of the pipe in the plane of the outlet. The response of the flow to a single pulse at different Reynolds numbers was studied by observing the traces recorded by these wires. Particular items noted were (i) the time required for a puff to move from station to station, (ii) the number of puffs crossing each station, (iii) the duration of the puffs at each station, and (iv) whether the hot wire positioned on the axis of the pipe provided visual evidence that the turbulent regions observed were indeed puffs.

For $Re < 2300$ a single disturbance of short duration gave rise to a single puff. It was relatively easy to identify such puffs and measure the time interval between their appearances at any two measuring stations. By assuming that the velocity of the trailing edge of a puff is independent of radial position (i.e. that

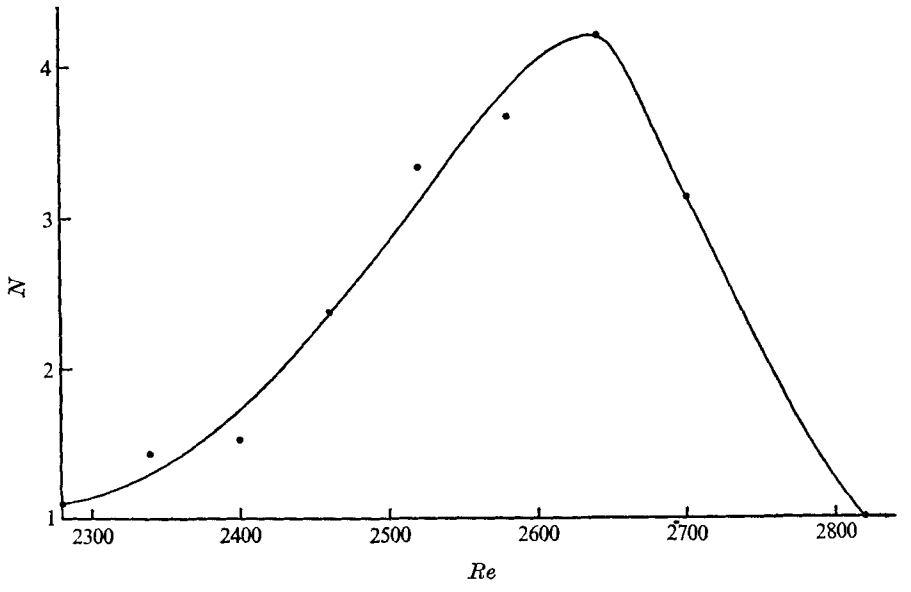

FIGURE 5. The effect of splitting: the number N of puffs resulting from a single disturbance.

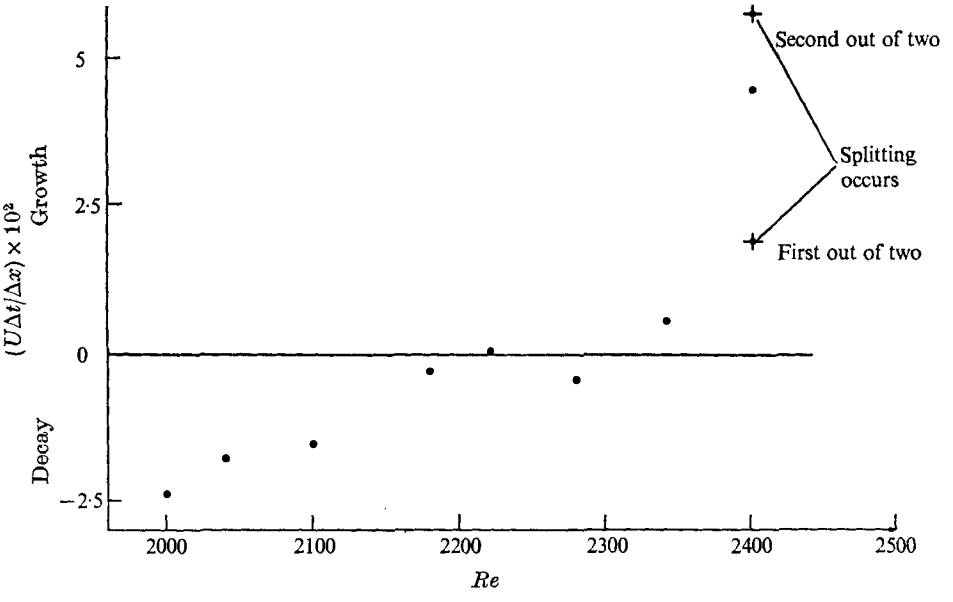

FIGURE 6. The effect of Reynolds number on the growth of a puff.

the shape of the trailing interface does not distort with downstream distance) the average propagation velocity of the puffs can be obtained.

Unfortunately this method did not yield satisfactory results for $2300 < Re < 2800$ because of splitting and growing of individual puffs. The average number of puffs at $x/D = 500$ resulting from a single pulse applied to the flow at $x/D = 50$

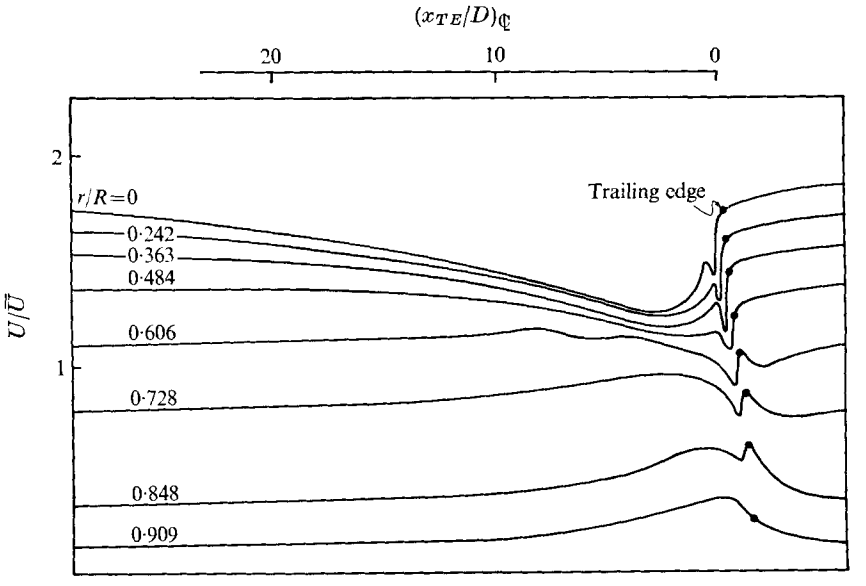

FIGURE 7. Time record of velocities.

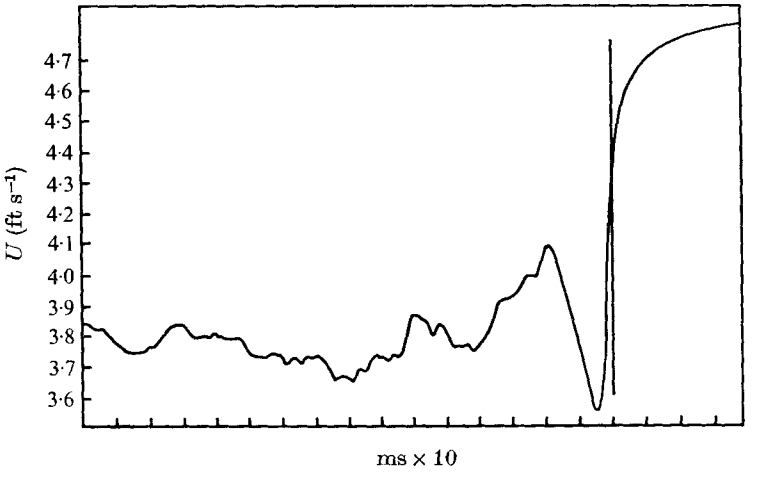

FIGURE 9. Time record of U near the interface.
Number of realizations = 101, r/R = 0·363.

is shown in figure 5. For $Re < 2300$ no splitting was observed. The average number of puffs increased with increasing Re for $Re > 2300$, resulting in a maximum of approximately four at $Re = 2600$. A further increase of Re decreased the number of puffs until at $Re \approx 2800$ a single slug-like turbulent region moving down the pipe was observed. It is not clear whether the decrease in the number of observable puffs occurred as a result of growth and recombination or very rapid successive splitting which does not allow the observer to distinguish between adjacent turbulent regions. Indeed some of the hot-wire signatures observed for $Re > 2600$ were no longer typical of turbulent puffs.

While examining the lengths of the puffs at each station we realized that they

grow with x for $Re > 2300$ and diminish with x for $Re < 2200$ (figure 6). The equilibrium puff, which should in principle maintain its length indefinitely, occurs for $2200 < Re < 2300$. The detailed measurements were thus made at $Re = 2200 + 20$. The effect of splitting on the growth of the puff is also shown in figure 6. In an array of two (which occurs quite often at $Re = 2400$), the leading puff lengthens slowly while the growth of the trailing puff is much more rapid. The total growth of the two puffs is approximately equal to the growth of a single puff at the same Re.

4.2. *The mean motion relative to the puff*

A set of ensemble-averaged time records of the mean velocity U at different radial locations in the pipe is shown in figure 7 (r is the distance from the pipe centre-line and R is the radius of the pipe). Each curve was produced using the cursor-alignment procedure described above.

In the central core of the pipe ($0 < r/R < 0{\cdot}5$), the velocity at a fixed station drops slowly as the puff approaches and then increases rapidly just before the passage of the trailing edge. The final rise, to a level which is only slightly below the velocity which prevails in the laminar zone, takes place in less than 0·005 s. The last turbulent fluctuation near the trailing interface is usually downwards (i.e. towards a lower velocity). The duration of this fluctuation is approximately 0·020 s (figure 2*b*), corresponding to a circular frequency of 25 Hz. For

$$0{\cdot}9 > r/R > 0{\cdot}6$$

the velocity increases in the forward, leading portion of the puff. This increase in velocity is accompanied by an increase in the turbulence level. Within the turbulent zone the velocity drops, reaching a minimum before the trailing interface. The last large turbulent fluctuation is again downwards (see figure 8, plate 3).

The fact that the predominant frequency and direction of these fluctuations are not random is reflected in the shape of the ensemble-averaged time records of U. An expanded computer output for 101 averaged realizations at $r/R = 0{\cdot}363$ is shown in figure 9. In spite of the fine time resolution and the absence of any smoothing, there is little doubt about the coherence of the signal near the interface. The slope of U near the trailing edge of the puff most probably represents a combination of (i) the actual deceleration of the flow at the trailing edge and (ii) error in precisely locating the interface. If we assume that a discontinuity in velocity is permitted across the interface (i.e. $\partial U/\partial t \rightarrow \infty$) we find that the maximum possible error in locating the interface does not exceed 0·003 s, which would correspond to a spatial resolution of 0·003 m. The coherence of the prevailing fluctuation disappears near the wall ($r/R \geqslant 0{\cdot}8$). Organized motion may still prevail at $r/R > 0{\cdot}8$ but our criterion for determining the trailing interface may not be applicable there. We are unable to say whether an interface exists in this region on the basis of visual observations, and it is possible that the interface does not extend all the way to the wall.

The earlier use of less sophisticated triggering methods caused a slight jitter in the marking of the interface, entirely obliterating the hump in the velocity

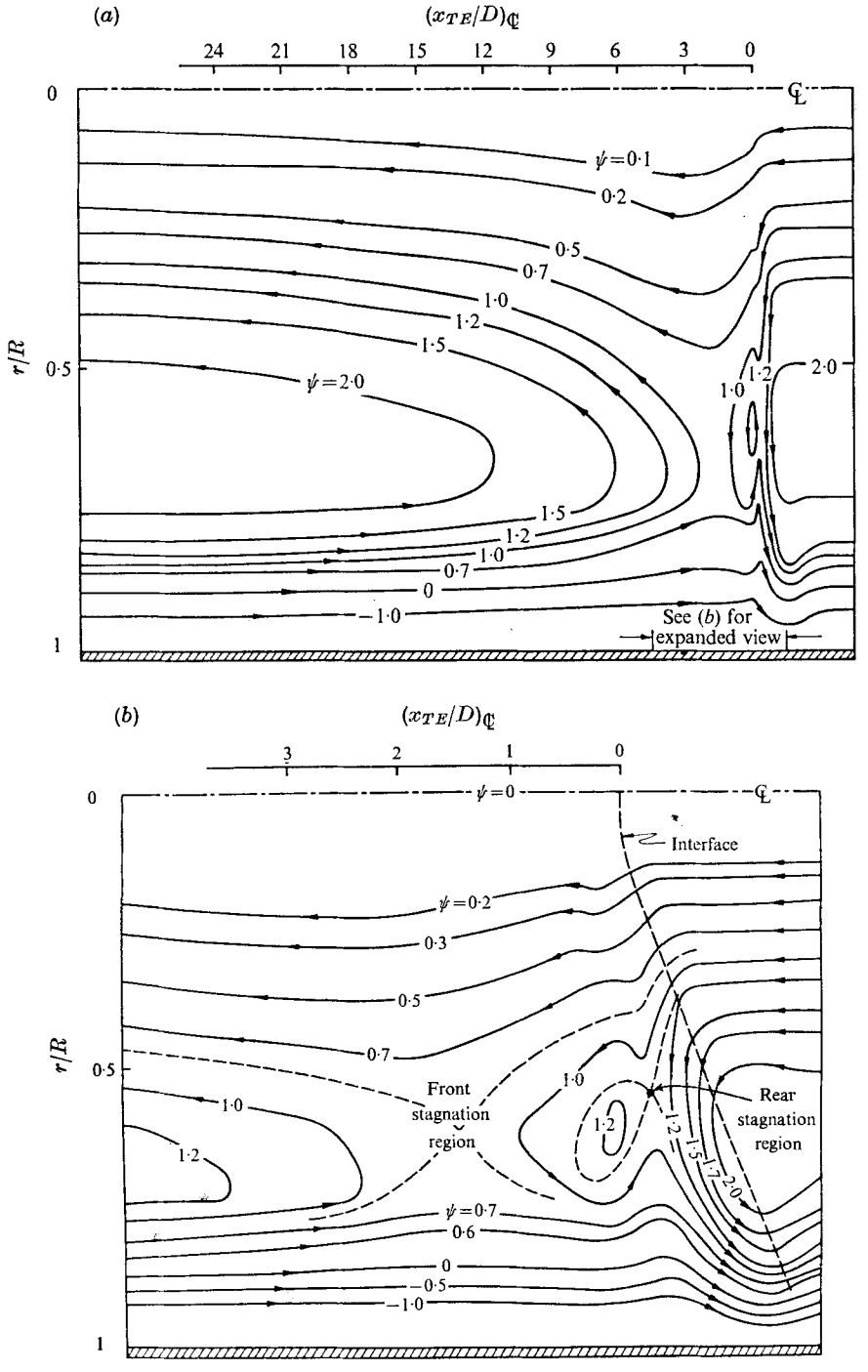

FIGURE 10. Streamline patterns in a puff.

records. To verify that the hump does not stem from the disturbance generator, we removed the speaker and placed an orifice plate at the inlet. The puffs appeared at random but when the velocity was recorded and the ensemble averages were obtained, the time records were identical to those shown in figures 7 and 9.

Cumulative histograms of the cursor locations relative to the on-axis reference probe were obtained as a by-product of the averaging process, as mentioned earlier. These were used to determine an average shape of the trailing interface of the puff. The interface appears to curve towards the rear with increasing distance from the centre-line. It is quite similar in shape to the interface of a slug (W & C), but somewhat more blunt (figure 10*b*).

Quasi-steady streamline patterns in a frame of reference moving with the trailing interface of the puff are shown in figures 10(*a*) and (*b*). Figure 10(*b*) is an expanded view of figure 10(*a*) near the trailing interface. The pattern resembles the schematic diagram suggested by Coles (1962); however, one should keep in mind that the radial scale in figure 10(*b*) is 10 times the axial scale. The puff consists of two large flattened ring vortices which rotate in the same direction and a small eddy in the vicinity of the rearward interface. Two stagnation points (rings) located approximately at $r/R = 0{\cdot}6$ separate the three vortices. The centre of the small eddy is also situated at $r/R = 0{\cdot}6$, in a plane which coincides with the turbulent interface on the centre-line of the pipe.

In the central stream tube in which, approximately, $0 \leqslant \psi \leqslant 0{\cdot}7$ (ψ is given in arbitrary units) the fluid overtakes the rearward interface. The flow decelerates in two stages as it becomes turbulent. Immediately after crossing the interface there is a strong, almost shock-like deceleration which is followed by a partial acceleration (i.e. relaxation). This cycle is approximately complete by the time the fluid has travalled 0·5 diameters from the interface. A much slower deceleration follows and terminates approximately two diameters from the trailing edge; from there on the fluid accelerates gradually until it leaves the puff. Near the wall ($\psi < 0{\cdot}7$) the reverse process occurs since the puff overtakes the fluid. The flow comes from the front and decelerates slowly relative to the puff. Before it reaches the rearward interface (at approximately one diameter from it) a much stronger deceleration occurs.

As the fluid passes the small toroidal eddy it experiences a strong acceleration until it leaves the puff through the rearward interface. The fluid which is bounded by $\psi > 1{\cdot}0$ on the left side of figure 10(*b*) enters the puff from the front, changes direction and leaves from the same side. The fluid for which $1{\cdot}2 < \psi < 2$ on the right-hand side of figure 10(*b*) crosses the interface in $0{\cdot}3 < r/R < 0{\cdot}5$, becomes turbulent and then leaves the puff by crossing the same interface again in $0{\cdot}75 < r/R < 0{\cdot}85$. The fluid for which $1{\cdot}0 < \psi < 1{\cdot}2$ also enters and leaves the puff through the rearward interface, however it also surrounds the small toroidal eddy in the process. There is some fluid in the eye of the small vortex which remains turbulent all the time.

The streamline pattern may give some explanation for the progressively poorer definition of the rearward interface with increasing r beyond $r/R = 0{\cdot}75$, and for the non-existence of a leading interface of the puff. We suggest that

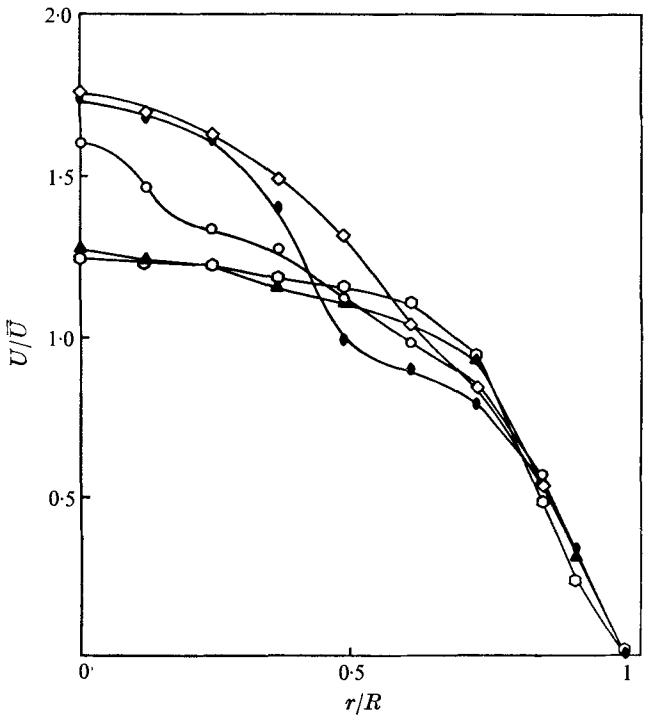

FIGURE 11. Radial distribution of mean velocity.

	0	▲	○	♦	◇
$(x_{TE}/D)_{\mathbb{C}}$	3·6	1·8	0	−0·6	−1·2

transition to turbulence in which random vorticity is produced occurs abruptly through an interface. The reverse process in which vortices are aligned, stretched and finally dissipated while the mean flow accelerates is much slower and hence cannot be restricted by an abrupt interface. We are unable to prove this statement but it is consistent with known previous observations. Both interfaces of the turbulent slug (W & C) are clearly defined, for they entrain laminar flow; all known free shear flows have a well-defined interface for they ingest irrotational fluid.

The radial distributions of velocity in the vicinity of the rearward interface are plotted in figure 11 (the distances from the interface are measured along the centre-line of the pipe). The cross-section chosen for the presentation of the first profile, $(x_{TE}/D)_{\mathbb{C}} = -1{\cdot}2$, lies outside the turbulent region for $r/R < 0{\cdot}75$ and inside the turbulent region at larger radial distances. Nevertheless the radial velocity distribution is typical of laminar flows. This is probably so because the turbulent fluid intercepted by the plane in which the velocity was measured is in a final process of relaminarization. The velocity profile at $(x_{TE}/D)_{\mathbb{C}} = -0{\cdot}6$ is outside the turbulent region for $r/R < 0{\cdot}43$. This profile has a strong change of slope in the vicinity of the interface. The profile at $(x_{TE}/D)_{\mathbb{C}} = 0$ is measured on the interface for $0 < r/R < 0{\cdot}1$; it too shows a rapid change in slope as the interface recedes from the plane of measurement. The other two profiles shown

in figure 11 were taken in the heart of the turbulent zone [$(x_{TE}/D)_{\mathbb{C}} = 1{\cdot}8$ and $3{\cdot}6$] and resemble the velocity distributions which exist in fully turbulent pipe flow at low Re.

It is interesting to note that the slopes of the velocity profiles near the wall, and hence the skin friction at the wall, are hardly affected by the presence or absence of turbulence.

Integration of the profiles shown in figure 11 indicates that the instantaneous mass flow did not remain constant during the passage of a puff. The largest difference occurred near the trailing interface, when the mass flow dropped by approximately 6%. There is no difference however between the mass flow in a laminar zone and the mass flow in a puff for $x_{TE}/D > 4$. The mass flow was measured independently by a flowmeter which did not deviate by more than 1% from its preset position. Although the flowmeter is a rather slow reacting instrument it had ample time to respond to the presence of a puff in the pipe (approximately 17 s). It is thus believed that a small error in the velocity near the wall of the pipe is responsible for the discrepancy in the mass flow.

4.3. *Turbulent intensities and Reynolds stress*

In figures 12(a)–(d) the three components of the turbulent intensity are plotted in contour form on the background of the streamline pattern. This presentation was chosen because it lends itself best to a physical interpretation although some quantitative accuracy of the data is lost.

The longitudinal fluctuations are most intense in the central region of the pipe near the trailing interface. The contours on the right-hand side of figure 12(a) are approximately parallel to the interface, yet it appears that some velocity fluctuations are imparted to the laminar zone. Although the laminar zone is not devoid of velocity fluctuations the intensity contours are somewhat shifted to the right as a result of the exponential decay in the filtering process and some errors in locating the interface. Further from the trailing interface inside the puff the intensity $u'^2/\overline{U}^2$ drops rather slowly. This drop in $u'^2/\overline{U}^2$ is particularly slow in $0{\cdot}4 < r/R < 0{\cdot}8$, where the residence time of the flow in the vicinity of the front stagnation point is approximately double that in the other regions. This is a direct result of the streamlines reversing their direction some three diameters from the trailing edge. Further acceleration of the flow leads to relaminarization. The change in the turbulent intensity is given in absolute terms because the intensities presented were rendered dimensionless by being normalized with respect to a constant velocity $\overline{U}$. Hence the available turbulent kinetic energy and Reynolds stress drop with increasing distance from the trailing edge and some kind of 'reverse-transition' occurs. This differs from the case of rapidly accelerated boundary layers, where the level of turbulent energy remains approximately constant in the presence of an ever-increasing mean velocity (Kovasznay 1971).

It is convenient to attribute the reduction in the turbulent intensity to the local acceleration of the mean flow. The stream tube $0 < \psi < 0{\cdot}7$ in the central region of the pipe has undergone an area contraction of 3·5 by the time the flow becomes fully laminar (see figure 10a). In the wall region near the trailing

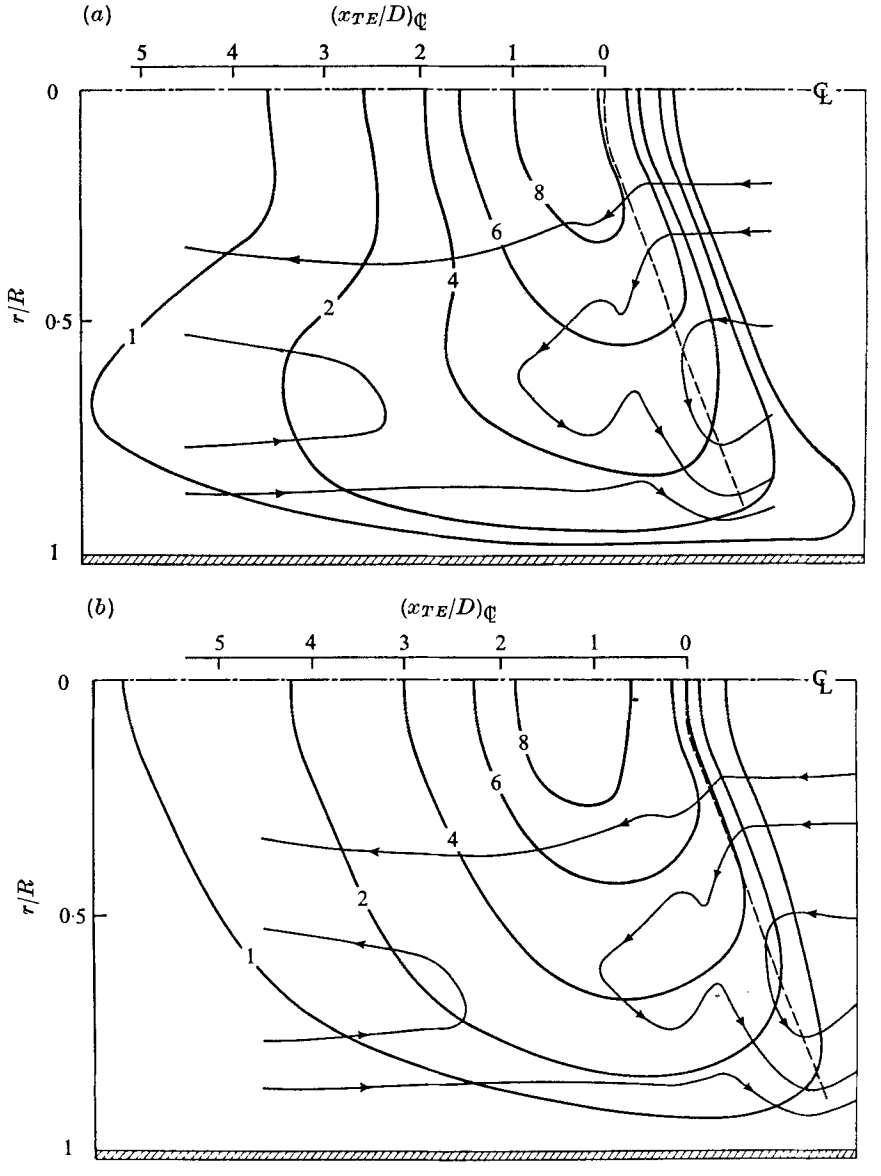

FIGURES 12(*a*) and (*b*). For legend see facing page.

interface the flow bounded by $\psi = 0{\cdot}7$ and the wall has undergone an area contraction of approximately 2 by the time it leaves the puff. Also, some of the longitudinal fluctuations which were captured by the small coherent eddy may be ejected outwards through the trailing edge. Thus the 'bulge' in the u'^2 contours near the wall may have resulted from the convection of turbulence towards the wall and outwards through the trailing edge of the puff.

The contours of the radial fluctuations v'^2 (figure 12*b*) differ only slightly from the contours of u'^2. In particular they lack the 'bulges' of the u'^2 contours near the trailing edge and the front of the puff. In both cases the restricted radial

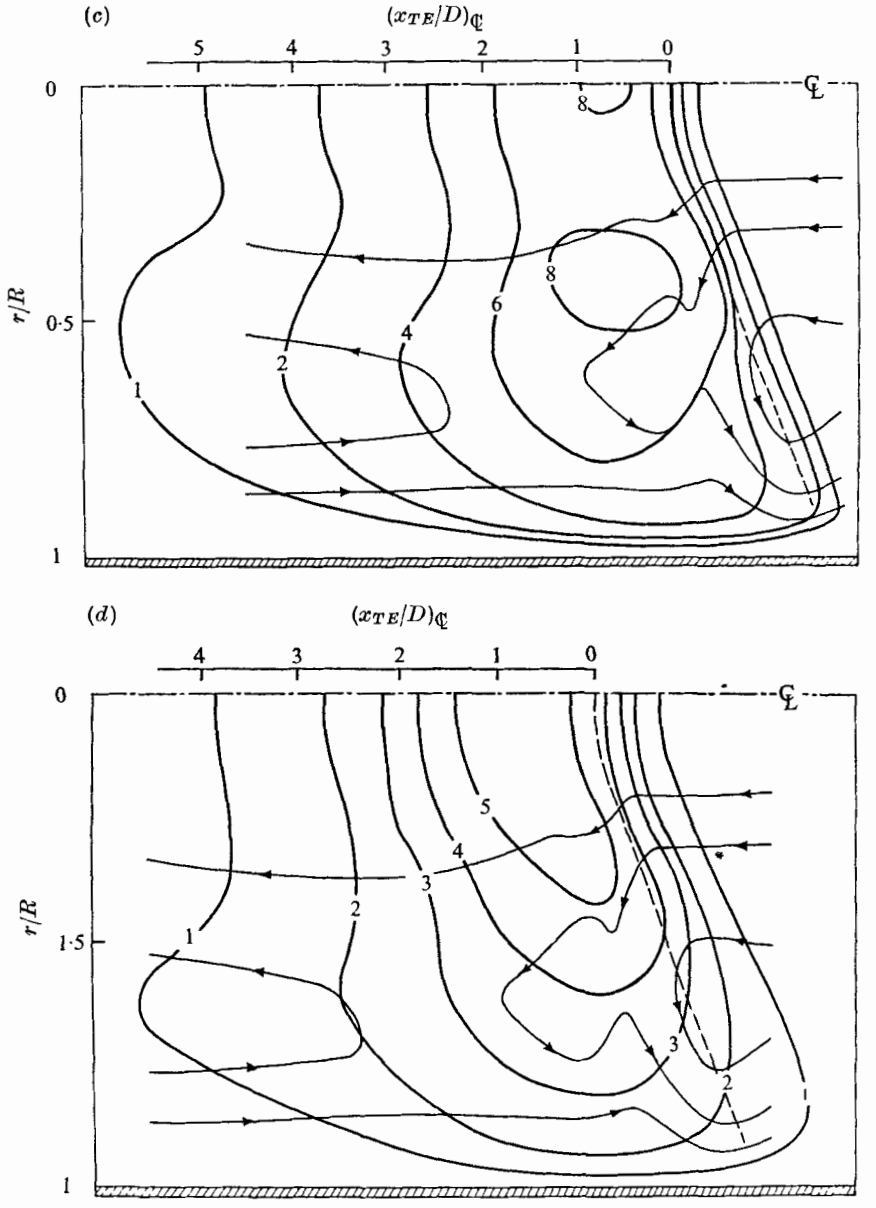

FIGURE 12. Contours of (*a*) $(u'^2/\overline{U}^2)\times 4{\cdot}4\times 10^{-3}$, (*b*) $(v'^2/\overline{U}^2)\times 1{\cdot}32\times 10^{-3}$, (*c*) $(w'^2/\overline{U}^2)\times 1{\cdot}32\times 10^{-3}$ and (*d*) $(q^2/\overline{U}^2)\times 10^{-2}$.

distance which is available in the stream tube under consideration may be too small for the prevailing radial fluctuations to maintain themselves.

The contours of the transverse fluctuations w'^2 (figure 12*c*) have two maxima: a small one on the centre-line of the pipe and a larger one at $r/R \approx 0{\cdot}4$ in the vicinity of the small toroidal eddy.

The total turbulent intensity $q^2 = u'^2+v'^2+w'^2$ is shown in figure 12(*d*) and some radial distributions of q^2 at various distances from the interface are shown

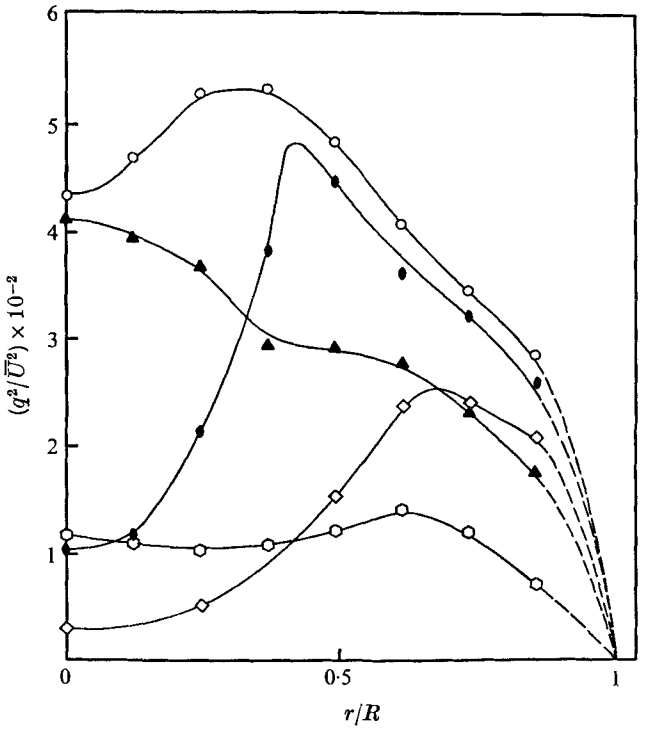

FIGURE 13. Radial distribution of turbulent energy. Symbols as in figure 11.

in figure 13. Since the intensity u'^2 is approximately equal to the sum of the intensities of the other two components the contours of q^2 resemble the contours of u'^2. In the central region of the pipe the turbulent intensity in the puff ($q/\bar{U} = 0{\cdot}22$) is four times larger than the intensity known to exist in the central region of a fully turbulent pipe flow. There is also a great difference in the distributions of q in those two flows. While in fully turbulent pipe flow q increases towards the wall, the opposite happens in the case of the turbulent puff. About three pipe diameters upstream from the trailing interface the puff resembles somewhat fully turbulent pipe flow at low Reynolds number and the radial distribution of the intensity (figure 13) has approximately the right magnitude and shape.

The contours of the Reynolds stress are shown in figure 14. The radial gradient of the turbulent shear stress is very large near the centre-line of the pipe, where $\overline{u'v'}$ vanishes. The region of maximum stress extends from $r/R = 0{\cdot}15$ to $r/R = 0{\cdot}4$ and is located axially where the flow recovers from the initial deceleration which it suffers as it crosses the interface. Within 3·5 diameters from the interface (i.e. at $(x_{TE}/D)_{\mathbb{C}} = 3{\cdot}5$) the maximum level of the Reynolds stress drops by an order of magnitude (figure 15). The Reynolds stress drops much faster with increasing distance from the interface than the intensity does. To illustrate this point we compare the maximum shear-stress correlation $R_{uv} = \overline{u'v'}/u'v'$ at four cross-sections in table 1.

The rapid decay of the shear stress reduces the production of turbulent energy

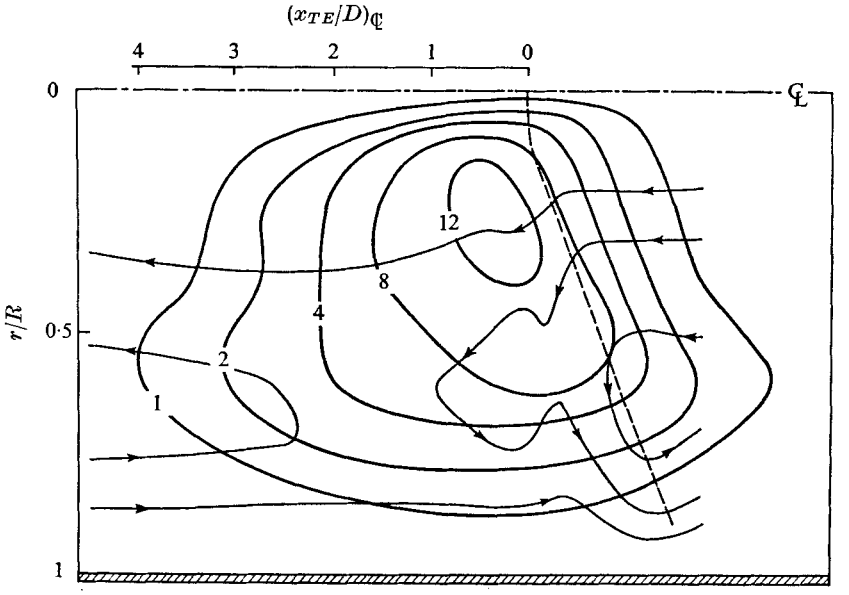

FIGURE 14. Contours of $(\overline{u'v'}/\overline{U}^2) \times 4{\cdot}4 \times 10^{-4}$.

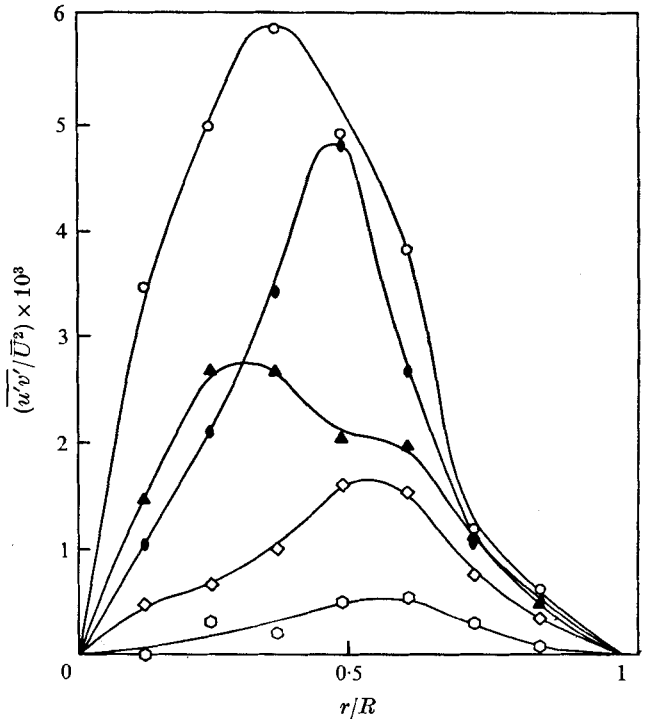

FIGURE 15. Radial distribution of Reynolds stress. Symbols as in figure 11.

$(x_{TE}/D)_{\mathbb{C}}$	0	1·5	3	4·5
R_{uv}	0·35	0·30	0·18	0·052

TABLE 1

and leads to the final deterioration of the turbulent puff. It should also be noted that R_{uv} never attains the level of 0·4 which is so well known in turbulent shear flows.

4.4. *Some energy considerations*

The contours shown in figure 16 represent the sum of the three digitally differentiated, squared and ensemble-averaged components of the velocity fluctuations. This can be shown to approximate the dissipation term. Taylor's hypothesis was assumed in making the transformation from temporal to spatial derivatives. (The velocity used in the transformation was the local ensemble-averaged value U.)

The dissipation terms do not attain their maxima close to the interface but further downstream. The dissipative scales always lag behind the energy-containing eddies in their development because some time is required for the cascade process to take effect. In the case of a puff the flow traverses approximately half a pipe diameter between the time at which the turbulent intensity attains its maximum and the time at which the dissipative eddies reach their peak values.

There appears to be an increase in the intensity level of the dissipative scales near the wall (figure 16). The contours of $U^{-2}(\partial u_i'/\partial t)^2$ must close near the surface but our measurements did not extend sufficiently close to the wall in order to draw them properly.

We have computed the energy budget at three cross-sections relative to the interface of the puff. The first cross-section is at $(x_{TE}/D)_{\mathbb{C}} = -0{\cdot}6$, the second at 0 and the third at 1·8. The vertical scale in the energy budget shown in figure 17 is identical at all of these cross-sections. The location of the first cross-section was chosen because it intercepts the turbulent interface at $r/R = 0{\cdot}4$, where it is in a field of strong radial velocity and just before the rearward stagnation point. The second cross-section coincides with the interface on the centre-line of the pipe; it is totally within the turbulent zone and passes through the middle of the small coherent eddy. This cross-section is located between the two stagnation points. The third cross-section passes through the front stagnation point (figure 17*a*).

The equations of the energy balance in the pipe in co-ordinates moving with an interface were derived for the turbulent slug in the first part of this investigation. All assumptions are still applicable for the puff with the exception of that concerning the production term, which is considered here in full:

$$2\left[(\overline{u'^2}-\overline{v'^2})\frac{\partial U}{\partial x}+(\overline{w'^2}-\overline{v'^2})\frac{V}{r}+\overline{u'v'}\left(\frac{\partial U}{\partial r}+\frac{\partial V}{\partial x}\right)\right].$$

Production by normal stresses — Production by Reynolds stresses

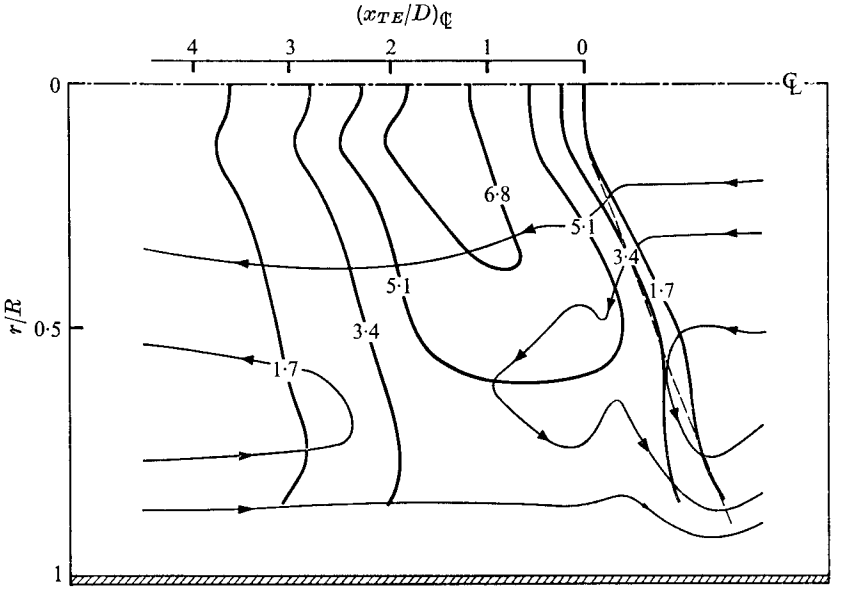

FIGURE 16. Contours of $6\nu R \times 10^3/\overline{U}^3\,[1/U^2/(\partial U_i'/\partial t)^2]$.

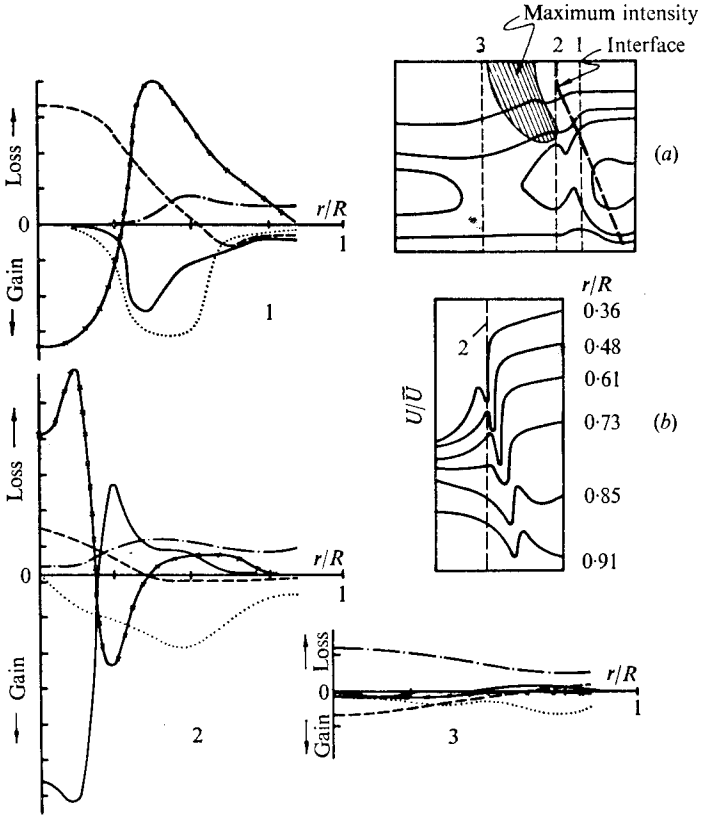

FIGURE 17. The energy budget near the interface. 1, $(x_{TE}/D)_{\mathbb{C}} = 0{\cdot}6$; 2, $(x_{TE}/D)_{\mathbb{C}} = 0$; 3, $(x_{TE}/D)_{\mathbb{C}} = 1{\cdot}8$. · · · · ·, production due to Reynolds stresses; ———, production due to normal stresses; – – –, convection; —·—, dissipation; —×—, diffusion.

The dissipation term increases from cross-section 1 to cross-section 3. At the first cross-section the dissipation vanishes for $0 \leqslant r/R \leqslant 0{\cdot}35$ because in this region the measurements were taken outside the turbulent interface. The dissipation is still very small at the second cross-section for $0 < r/R < 0{\cdot}12$, where the average location of the interface coincides with the plane of measurement. The third cross-section, however, is dominated by dissipation.

Turbulent energy is convected away from the trailing interface (towards the front of the puff) by the mean flow in the centre of the pipe and in the opposite direction near the wall. Energy is lost when convection occurs against the gradient of intensity, as in the central region of the pipe at cross-sections 1 and 2, and near the wall at cross-section 3. For $r/R > 0{\cdot}55$ at cross-section 1 the flow direction coincides with that of the intensity gradient and the convection term changes sign. At cross-section 2 the convection term almost vanishes for $r/R > 0{\cdot}35$ because the convective velocity is very small.

The production of turbulent energy was subdivided into two components: (*a*) production resulting from Reynolds stresses; (*b*) production resulting from normal stresses. The latter term is often neglected in turbulent shear flows for which the boundary-layer approximation applies, or in other flows which are assumed to be isotropic.

Since the gain of energy by shear production depends on the radial gradient of the velocity profile and on the $\overline{u'v'}$ correlation the production is highest between $r/R = 0{\cdot}3$ and $r/R = 0{\cdot}6$ in the vicinity of the turbulent interface (cross-sections 1 and 2). At cross-section 3, where the velocity profile is very flat over most of the cross-section (figure 11), maximum shear production is attained near the wall, where the intensity of $\overline{u'v'}$ is rather low (figure 14). There is an obvious mismatch in the radial locations of the two components contributing to the shear production. In fully turbulent pipe flow $\overline{u'v'}$ increases linearly with r over most of the pipe's cross-section. Thus, large values of $\overline{u'v'}$ coincide with relatively large values of $\partial U/\partial r$, leading to strong production which sustains the turbulent flow indefinitely.

The production of turbulent energy by normal stresses near the interface is not only of the same order of magnitude as the production by Reynolds stresses but even exceeds it. The first coherent turbulent fluctuation near the interface of the puff contributes to a velocity gradient $\partial U/\partial x$ which is not negligible with respect to $\partial U/\partial r$. When this effect is coupled with a strong anisotropy in which $u'^2 \approx 2v'^2$ it results in vigorous production of turbulent energy.

The flow which crosses cross-section 1 in $0 < r/R < 0{\cdot}7$ undergoes a deceleration which results in an overall gain of energy. At the second cross-section the flow decelerates near the centre ($0 \leqslant r/R \leqslant 0{\cdot}15$) and energy is gained by normal stress production. However, for $r/R > 0{\cdot}18$ the fluid starts to accelerate (see figure 17*b*) and the product $(u'^2 - v'^2)\,\partial U/\partial x$ contributes to a loss of turbulent energy. At times the loss of energy by 'normal stress production' outweighs the gain of energy through the customary product $\overline{u'v'}\,\partial U/\partial r$. We thus have a case of turbulent energy being extracted from the fluid by the mean motion. Negative production resulting from normal stresses occurs whenever the flow is accelerated

rapidly, however it is usually small compared with the production associated with shear.

A conjecture as to the mechanism of splitting at slightly higher *Re* may now be made. Strong negative production which occurs half a diameter to the left of the interface and parallel to it may momentarily quench all smaller fluctuations between the large rearmost eddy and the first coherent eddy inside the turbulent puff, causing them to separate. The small coherent eddy replaces the rearward large eddy in the truncated puff. For some time after separation the entrainment of laminar fluid by the trailing interface of the leading puff is inhibited by the presence of the separated large eddy in the neighbourhood. Thus, in an array of two puffs the growth of the leading puff should be slower than the growth of the trailing puff. Preliminary evidence of this effect is shown in figure 6. An incipient separation on the centre-line of the pipe is shown in figure 18 (plate 4), where the most rearward fluctuation is separated from the rest of the puff by 0·020 s of relatively calm fluid.

5. Concluding remarks

Rudimentary measurements were made in equilibrium puffs in order to gain some insight into the mechanism of transition in a pipe at low *Re*. In attempting to define the bounds of a puff we immediately face a difficulty because a puff has only one turbulent/non-turbulent interface at its trailing edge and even that is not clearly defined at large radial distances from the centre. A turbulent slug, on the other hand, is bounded by two well-defined interfaces spanning the entire cross-section of the pipe. The fluid crossing the rear interface of a slug proceeds inwards in a predominantly axial direction. The fluid which overtakes the rear interface of a puff may reverse its direction and leave the puff through the same 'interface' but closer to the wall of the pipe. Thus, in co-ordinates moving with a puff the boundary-layer assumptions are not applicable. The most intense turbulent fluctuations in a puff occur in the central region of the pipe near the interface. Since the production of turbulent energy depends in part on the product of the normal stresses and the axial gradient of the mean velocity it is limited to a very small region near the interface. Furthermore, it is possible to have a region in which the production and the dissipation have the same sign. Under these conditions the usual production term actually removes energy from the turbulence and transfers it to the mean motion. Because the total turbulent production is rather limited it all occurs in a small space near the trailing interface. The overall length of a puff (figure 10*a*) is most probably determined by the dissipation rate and hence by the small eddies. The result is that all puffs at a given Reynolds number are approximately of equal length.

REFERENCES

BRESLIN, J. A. 1970 *Lehigh University Tech. Rep.* no. 22.

COLES, D. 1962 *Mécanique de la Turbulence* (ed. Favre), p. 229. Paris: C.N.R.S.

KOVASZNAY, L. S. G. 1971 *AGARD Specialists Meeting on Turbulent Shear Flow*, reprint no. 93.

LINDGREN, E. R. 1957 *Arkiv Fys.* **12**, 1–169.

VALERANI, E. 1964 Engineers thesis, Guggenheim Aero. Lab., California Institute of Technology.

WYGNANSKI, I. J. & CHAMPAGNE, F. H. 1973 *J. Fluid Mech.* **59**, 281–335.

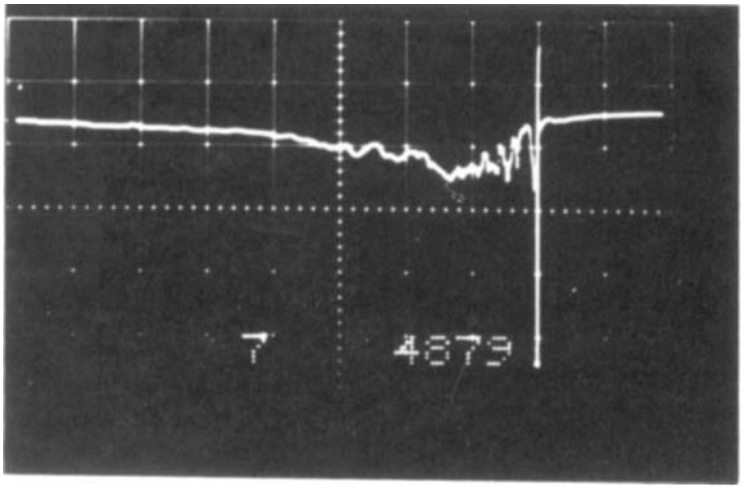

(*a*)

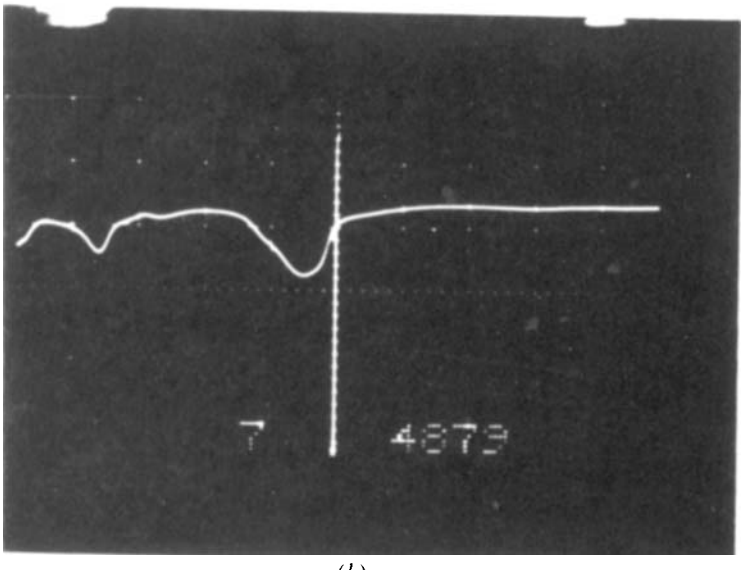

(*b*)

FIGURE 2. The determination of the trailing interface by the cursor program. The first number indicates the number of the puff in the ensemble. The second number indicates the location of the trailing front. (*a*) An oscilloscope trace of the entire puff. (*b*) Expanded near the trailing edge.

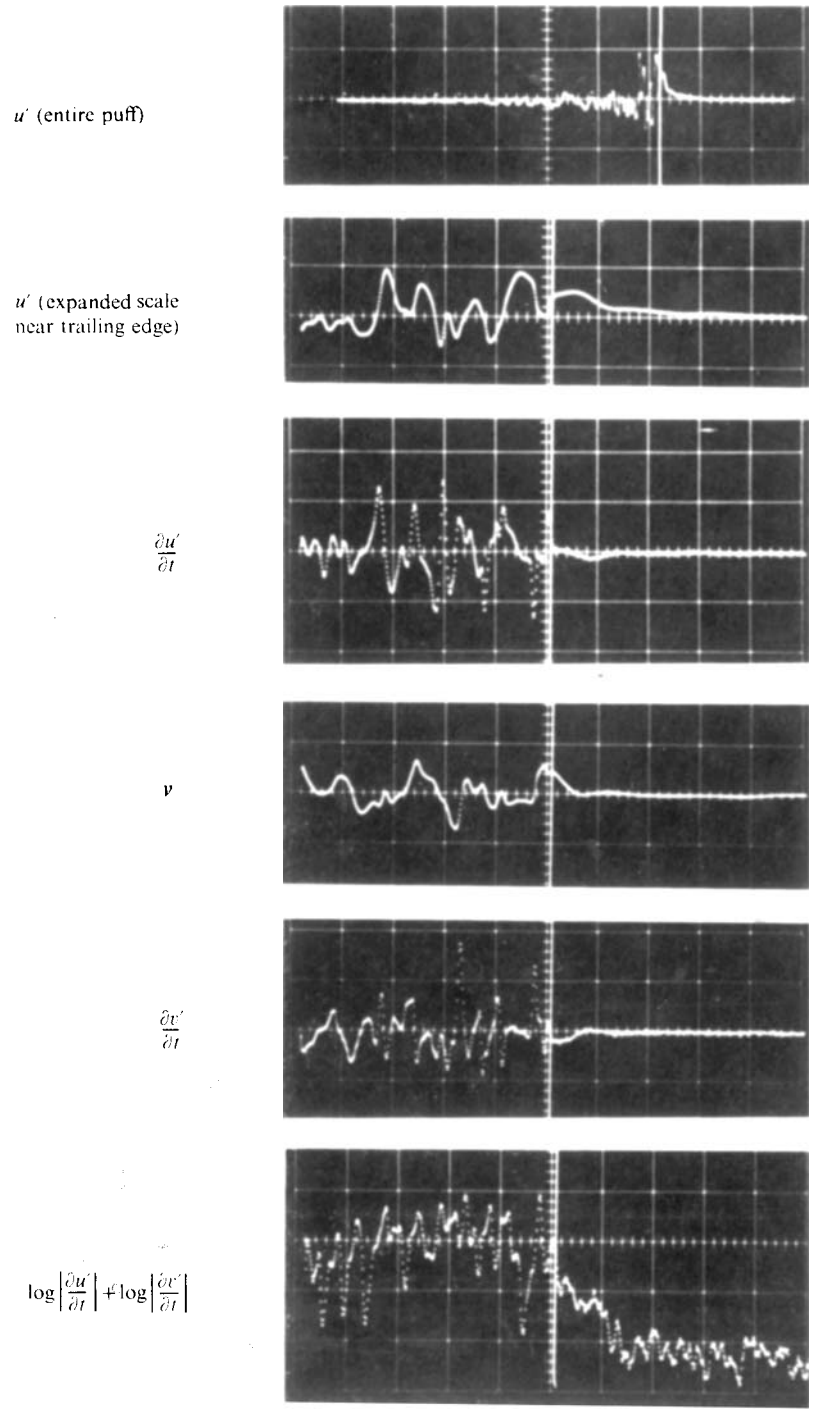

FIGURE 3. X-wire traces near the trailing interface.

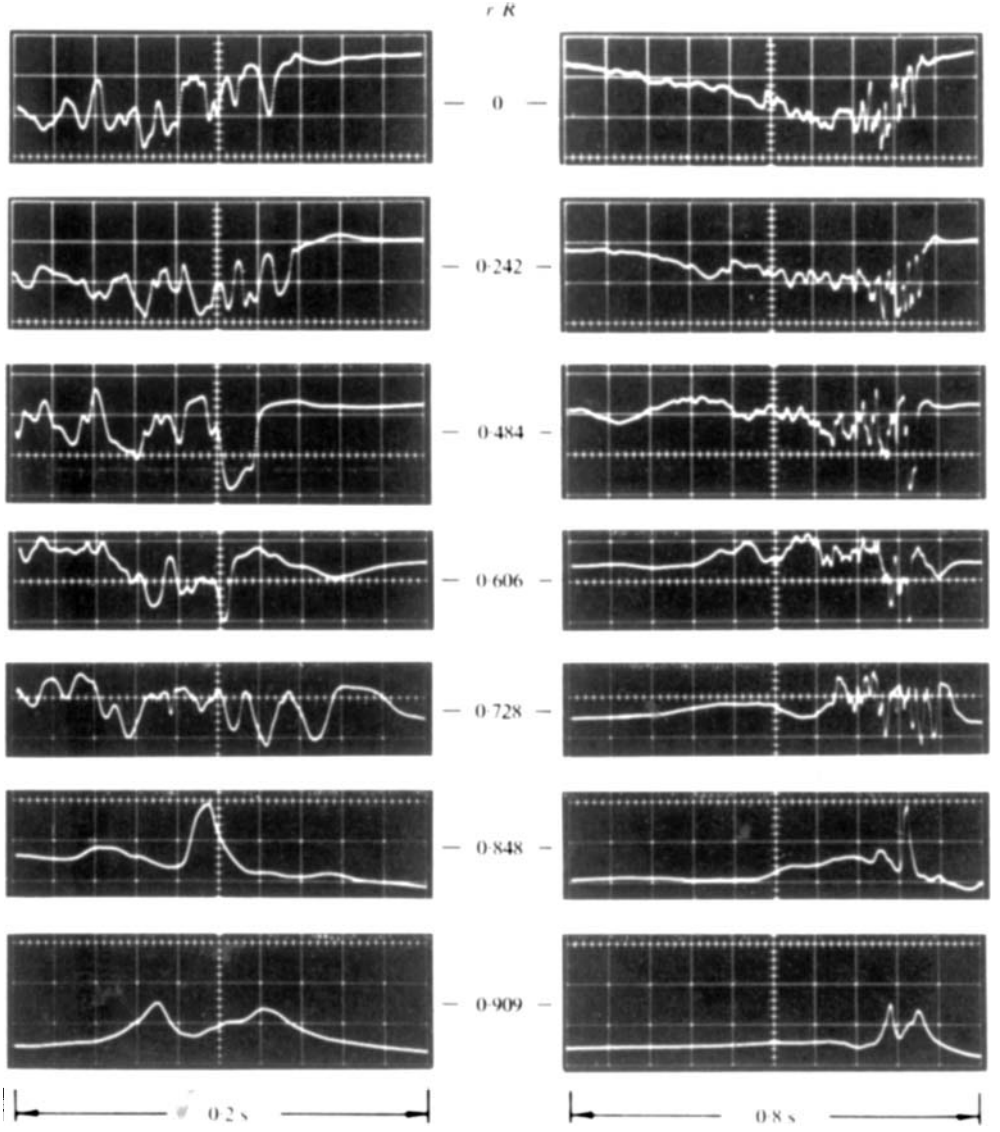

FIGURE 8. Hot-wire traces of velocities at various radial locations in a pipe. Vertical scale: 1 division = 2 ft s^{-1}.

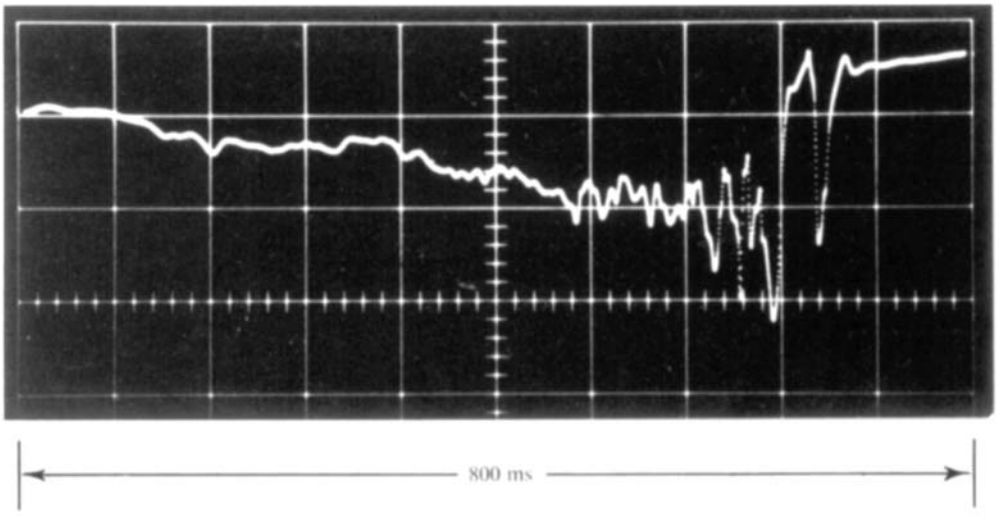

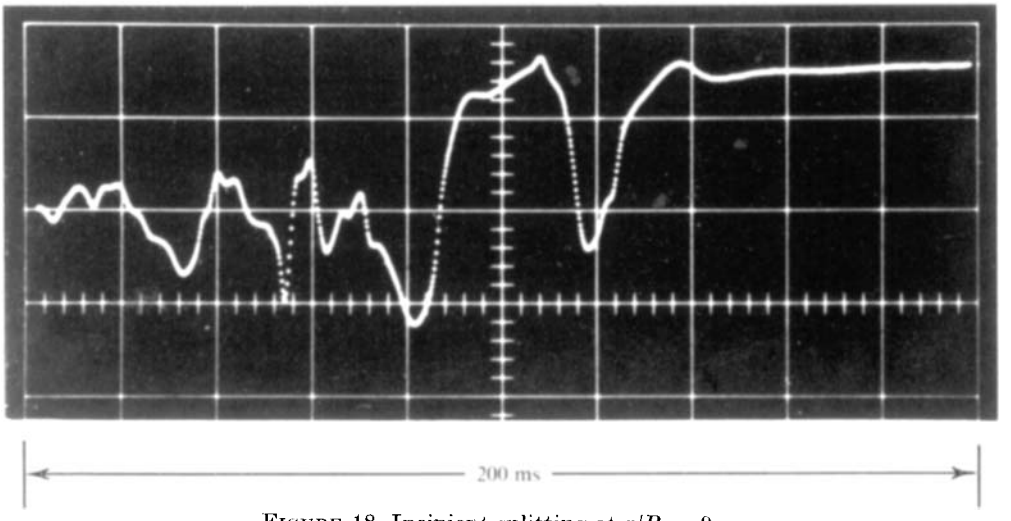

FIGURE 18. Incipient splitting at $r/R = 0$.